

THE FIRST THREE POMERONS...

V. A. PETROV^{a,1} and A. V. PROKUDIN^{a,b,2}

(a) *Institute For High Energy Physics,
142281 Protvino, RUSSIA*

(b) *Dipartimento di Fisica Teorica,
Università Degli Studi Di Torino,
Via Pietro Giuria 1, 10125 Torino,
ITALY
and
Sezione INFN di Torino,
ITALY*

A model of a three Pomeron contribution to high energy elastic pp and $\bar{p}p$ scattering is proposed. The data are well described for all momenta ($0.01 \leq |t| \leq 14. \text{GeV}^2$) and energies ($8. \leq \sqrt{s} \leq 1800. \text{GeV}$) ($\chi^2/\text{d.o.f.} = 2.74$). The model predicts the appearance of two dips in the differential cross-section which will be measured at LHC. The parameters of the Pomeron trajectories are:

$$\begin{aligned} \alpha(0)_{\mathbb{P}_1} &= 1.058, \quad \alpha'(0)_{\mathbb{P}_1} = 0.560 \text{ (GeV}^{-2}\text{)}; \\ \alpha(0)_{\mathbb{P}_2} &= 1.167, \quad \alpha'(0)_{\mathbb{P}_2} = 0.273 \text{ (GeV}^{-2}\text{)}; \\ \alpha(0)_{\mathbb{P}_3} &= 1.203, \quad \alpha'(0)_{\mathbb{P}_3} = 0.094 \text{ (GeV}^{-2}\text{)}. \end{aligned}$$

1 INTRODUCTION

Fervently awaited high-energy collisions at LHC will give an access not only to yet unexplored small distances but also simultaneously to neither explored large distances [1]. Future measurements of total and elastic cross-sections at LHC [2] tightly related to the latter domain naturally stimulate further searches for new approaches to diffractive scattering at high energies.

Recently some models with multi-Pomeron structures were proposed [3, 4, 5]. Some of them [3], [4] use Born amplitudes with two Pomerons as single [3] or double poles [4]. Formal violation of the Froissart-Martin bound

¹*E-mail:* petrov@mx.ihep.su

²*E-mail:* prokudin@to.infn.it

in some of these models is considered as “practically negligible” though in terms of parial-wave amlitudes unitarity violation is flagrant at present-day energies. Nonetheless a model of such kind [5] based on the two-Pomeron approach shows quite a good agreement with DIS data.

The eikonal models that are capable of describing the data for nonzero transferred momenta are developed in Refs [6], [7]. In some cases a “generalized eikonal representation” is used [6] together with a dipole (monopole) Pomeron contibution, in the others the conventional eikonal is supplemented with a “QCD motivated” part consisting of three terms [7]. It is worth noticing that the two-Pomeron eikonal has been applied to the description of the data more than ten years ago (see, e.g., Ref. [8]).

The very multiformity of the models hints that maybe the most general way to describe high-energy diffraction is just to admit an arbitrary number of Pomerons (i.e. all vacuum Regge-poles contributing non-negligibly at reasonably high energies. Roughly, they should have intercepts not lower than 1). On the one hand this seems not very economical. But on the other hand we could argue that no basic principle forbids more than one single Pomeron. We could also add that in the perturbative framework the account of the renormalization group leads presumably to converting of the fixed branch point (in the J -plane) into an infinite series of simple poles accumulating down to 1 from some maximal value [9]. Unfortunately perturbative searches in this field are far from being satisfactory from many viewpoints.

In this paper we would like to make a first step in realization of the above formulated hypothesis about many-Pomeron structure of the eikonal. As it seems not possible to describe the data in the framework of the eikonal approach with presence of one single pole Pomeron contribution [10], and the two-Pomeron option does not improve quality of description drastically (more details are given in the text) it is fairly natural to try the next, three-Pomeron, option for the eikonal. We will see below that this choice appears rather lucky.

2 THE MODEL

Let us briefly outline the basic properties of our model. Unitarity condition:

$$\Im m T(s, \vec{b}) = |T(s, \vec{b})|^2 + \eta(s, \vec{b}) ,$$

where $T(s, \vec{b})$ is the scattering amplitude in the impact representation, \vec{b} is the impact parameter, $\eta(s, \vec{b})$ is the contribution of inelastic channels, implies the following eikonal form for the scattering amplitude $T(s, \vec{b})$

$$T(s, \vec{b}) = \frac{e^{2i\delta(s, \vec{b})} - 1}{2i}, \quad (1)$$

where $\delta(s, \vec{b})$ is the eikonal function. The unitarity condition in terms of the eikonal looks as follows

$$\Im m \delta(s, \vec{b}) \geq 0, \quad s > s_{\text{inel}}. \quad (2)$$

The eikonal function is assumed to have simple poles in the complex J -plane and the corresponding Regge trajectories are normally being used in the linear approximation

$$\alpha(t) = \alpha(0) + \alpha'(0)t. \quad (3)$$

Accordingly we get the following (modulo the signature factor) contribution to the eikonal function in t -space (here t is the momentum transfer)

$$\hat{\delta}(s, t) = \frac{c}{s_0} \left(\frac{s}{s_0} \right)^{\alpha(0)} e^{t \frac{\rho^2}{4}}, \quad (4)$$

where

$$\rho^2 = 4\alpha'(0) \ln \frac{s}{s_0} + r^2 \quad (5)$$

is referred to as the “Reggeon radius”.

In order to relate t - and b -spaces one proceeds via Fourier-Bessel transforms

$$\begin{aligned} \hat{f}(t) &= 4\pi s \int_0^\infty db^2 J_0(b\sqrt{-t}) f(b), \\ f(b) &= \frac{1}{16\pi s} \int_{-\infty}^0 dt J_0(b\sqrt{-t}) \hat{f}(t). \end{aligned} \quad (6)$$

Making use of Eq. (6) we obtain the following b -representation of the eikonal function (4)

$$\delta(s, b) = \frac{c}{s_0} \left(\frac{s}{s_0} \right)^{\alpha(0)-1} \frac{e^{-\frac{b^2}{\rho^2}}}{4\pi\rho^2}. \quad (7)$$

For the cross-sections we use the following normalizations:

$$\begin{aligned}
\sigma_{tot} &= \frac{1}{s} \Im m T(s, t=0), \\
\sigma_{elastic} &= 4\pi \int_0^\infty db^2 |T(s, b)|^2, \\
\frac{d\sigma}{dt} &= \frac{|T(s, t)|^2}{16\pi s^2}, \\
\rho &= \frac{\Re e T(s, t=0)}{\Im m T(s, t=0)}.
\end{aligned} \tag{8}$$

In the present model we assume the following representation for the eikonal function:

$$\delta_{pp}^{\bar{p}p}(s, b) = \delta_{\mathbb{P}_1}^+(s, b) + \delta_{\mathbb{P}_2}^+(s, b) + \delta_{\mathbb{P}_3}^+(s, b) \mp \delta_{\mathbb{O}}^-(s, b) + \delta_f^+(s, b) \mp \delta_\omega^-(s, b), \tag{9}$$

here $\delta_{\mathbb{P}_{1,2,3}}^+(s, b)$ are Pomeron contributions. ‘+’ denotes C even trajectories (the Pomeron trajectories have the following quantum numbers $0^+ J^{++}$), ‘-’ denotes C odd trajectories, $\delta_{\mathbb{O}}^-(s, b)$ is the Odderon contribution (the Odderon is the C odd partner of the Pomeron with quantum numbers $0^- J^{--}$); $\delta_f^+, \delta_\omega^-(s, b)$ are the contributions of secondary Reggeons, f ($C = +1$) and ω ($C = -1$).

The form (4) is not compatible with analyticity and crossing symmetry, which are easily restored by substitution $s \rightarrow se^{-i\pi/2}$. We introduce a new dimensionless variable

$$\tilde{s} = \frac{s}{s_0} e^{-i\frac{\pi}{2}}, \tag{10}$$

and obtain each $C+$ and $C-$ contribution with its appropriate signature factor and the form:

$$\begin{aligned}
\delta^+(s, b) &= i \frac{c}{s_0} \tilde{s}^{\alpha(0)-1} \frac{e^{-\frac{b^2}{\rho^2}}}{4\pi\rho^2}, \\
\rho^2 &= 4\alpha'(0) \ln \tilde{s} + r^2, \\
(C = +1) ;
\end{aligned} \tag{11}$$

$$\begin{aligned}\delta^-(s, b) &= \frac{c}{s_0} \tilde{s}^{\alpha(0)-1} \frac{e^{-\frac{b^2}{\rho^2}}}{4\pi\rho^2}, \\ \rho^2 &= 4\alpha'(0) \ln \tilde{s} + r^2, \\ (C &= -1).\end{aligned}\tag{12}$$

The parameters of secondary Reggeon trajectories are fixed according to the parameters obtained from a fit of the meson spectrum [11]:

$$\begin{aligned}\alpha_f(t) &= 0.69 + 0.84t, \\ \alpha_\omega(t) &= 0.47 + 0.93t.\end{aligned}\tag{13}$$

All the trajectories are taken in linear approximation:

$$\alpha_i(t) = \alpha_i(0) + \alpha'_i(0)t, \quad (i = \mathbb{P}_1, \mathbb{P}_2, \mathbb{P}_3, \mathbb{O}).\tag{14}$$

Let us remark that all good fits require $\alpha_{\mathbb{P}}(0) - 1 \equiv \Delta_{\mathbb{P}} > 0$ which means that Born amplitude will eventually exceed the Froissart-Martin [12] unitarity bound. This violation of unitarity is removed by all kinds of “eikonalization”. Nevertheless, one must take into account the following unitarity constrains [13]

$$\alpha_{\mathbb{P}}(0) \geq \alpha_{\mathbb{O}}(0) \text{ and } \alpha'_{\mathbb{P}}(0) \geq \alpha'_{\mathbb{O}}(0),\tag{15}$$

there \mathbb{P} in this case is the leading Pomeron trajectory (the one with the highest intercept $\Delta_{\mathbb{P}}$).

3 RESULTS

We fitted the adjustable parameters over a set of 961 pp and $\bar{p}p$ data of both forward observables (total cross-sections σ_{tot} , and ρ – ratios of real to imaginary part of the amplitude) in the range $8. \leq \sqrt{s} \leq 1800. \text{GeV}$ and angular distributions ($\frac{d\sigma}{dt}$) in the ranges $23. \leq \sqrt{s} \leq 1800. \text{GeV}$, $0.01 \leq |t| \leq 14. \text{GeV}^2$.

Having used 20 adjustable parameters we achieved $\chi^2/\text{d.o.f.} = 2.74$. The parameters are presented in Table 1 (all the errors are obtained according to MINUIT output).

	Pomeron₁		f-Reggeon
$\Delta_{\mathbb{P}_1}$	0.0578 ± 0.0020	Δ_f	-0.31 (FIXED)
$c_{\mathbb{P}_1}$	53.007 ± 0.795	c_f	191.69 ± 2.12
$\alpha'_{\mathbb{P}_1}$	0.5596 ± 0.0078 (GeV^{-2})	α'_f	0.84 (GeV^{-2}) (FIXED)
$r_{\mathbb{P}_1}^2$	6.3096 ± 0.2522 (GeV^{-2})	r_f^2	31.593 ± 1.099 (GeV^{-2})
	Pomeron₂		ω-Reggeon
$\Delta_{\mathbb{P}_2}$	0.1669 ± 0.0012	Δ_ω	-0.53 (FIXED)
$c_{\mathbb{P}_2}$	9.6762 ± 0.1600	c_ω	-174.18 ± 2.72
$\alpha'_{\mathbb{P}_2}$	0.2733 ± 0.0056 (GeV^{-2})	α'_ω	0.93 (GeV^{-2}) (FIXED)
$r_{\mathbb{P}_2}^2$	3.1097 ± 0.1817 (GeV^{-2})	r_ω^2	7.467 ± 1.083 (GeV^{-2})
	Pomeron₃		
$\Delta_{\mathbb{P}_3}$	0.2032 ± 0.0041	s_0	1.0 (GeV^2) (FIXED)
$c_{\mathbb{P}_3}$	1.6654 ± 0.0669		
$\alpha'_{\mathbb{P}_3}$	0.0937 ± 0.0029 (GeV^{-2})		
$r_{\mathbb{P}_3}^2$	2.4771 ± 0.0964 (GeV^{-2})		
	Odderon		
$\Delta_{\mathbb{O}}$	0.19200 ± 0.0025		
$c_{\mathbb{O}}$	0.0166 ± 0.0022		
$\alpha'_{\mathbb{O}}$	0.048 ± 0.0027 (GeV^{-2})		
$r_{\mathbb{O}}^2$	0.1398 ± 0.0570 (GeV^{-2})		

Table 1: Parameters obtained by fitting to the data.

In order to estimate the quality of the description, we have calculated partial χ^2 over all sets of data used in the fit. This χ^2 is calculated using the following formula:

$$\chi^2 = \sum_{n=1}^{ntot} \frac{(\sigma_{theory}(n) - \sigma_{exp}(n))^2}{(\Delta(\sigma_{exp}(n)))^2}, \quad (16)$$

where $ntot$ is the number of data in the set, σ_{exp} is the experimental value of the quantity that is described, σ_{theory} is our prediction for this quantity, and $\Delta(\sigma_{exp}(n))$ is the experimental uncertainty.

The partial χ^2 may be found in Table 2.

	Set of data	Number of points, ntot	χ^2/ntot
1	$\sigma_{total}^{\bar{p}p}$	42	2.3524
2	σ_{total}^{pp}	50	0.6309
3	$\rho^{\bar{p}p}$	11	0.6942
4	ρ^{pp}	36	1.9075
5	$\frac{d\sigma}{dt}^{\bar{p}p}$, $\sqrt{s} = 31. (GeV)$	22	3.3688
6	$\frac{d\sigma}{dt}^{\bar{p}p}$, $\sqrt{s} = 53. (GeV)$	52	8.5457
7	$\frac{d\sigma}{dt}^{\bar{p}p}$, $\sqrt{s} = 62. (GeV)$	23	1.8524
8	$\frac{d\sigma}{dt}^{\bar{p}p}$, $\sqrt{s} = 546. (GeV)$	78	3.8425
9	$\frac{d\sigma}{dt}^{\bar{p}p}$, $\sqrt{s} = 630. (GeV)$	19	9.9273
10	$\frac{d\sigma}{dt}^{\bar{p}p}$, $\sqrt{s} = 1800. (GeV)$	51	1.3741
11	$\frac{d\sigma}{dt}^{pp}$, $\sqrt{s} = 23.5 (GeV)$	105	2.2491
12	$\frac{d\sigma}{dt}^{pp}$, $\sqrt{s} = 27.43 (GeV)$	39	1.8929
13	$\frac{d\sigma}{dt}^{pp}$, $\sqrt{s} = 30.7 (GeV)$	92	4.4559
14	$\frac{d\sigma}{dt}^{pp}$, $\sqrt{s} = 44.64 (GeV)$	97	1.5748
15	$\frac{d\sigma}{dt}^{pp}$, $\sqrt{s} = 52.8 (GeV)$	93	2.0956
16	$\frac{d\sigma}{dt}^{pp}$, $\sqrt{s} = 62. (GeV)$	151	2.4272
	Number of parameters	Total number of points	$\chi^2/\text{d.o.f.}$
	20	961	2.7441

Table 2: Partial χ^2 .

Some of these χ^2 s are high (for instance those for differential cross sections at $\sqrt{s} = 53, 630 \text{ GeV}$). It reflects the fact that we did not make use of systematical errors for these sets of data which can be as high as 30%.

The results are shown in fig. 1, 2, 3, 4, 5, 6, 7, 8.

We do not include elastic cross-section data sets into the fit and predictions of the model for elastic cross-sections can be seen in fig. 2.

It is instructive to compare these results with a two-Pomeron option. We give corresponding results in fig. 9, 10, 11, 12, 13. In this case $\chi^2/\text{d.o.f.} = 10.87$ what can be considered as an argument in favour of our hypothesis of many Pomerons. The parameters obtained in the two-Pomeron option are presented in Table 3 (all the errors are obtained according to MINUIT output).

	Pomeron₁		f-Reggeon
$\Delta_{\mathbb{P}_1}$	0.0859 ± 0.0021	Δ_f	-0.31 (FIXED)
$c_{\mathbb{P}_1}$	53.18 ± 0.86	c_f	188.51 ± 12.13
$\alpha'_{\mathbb{P}_1}$	$0.360 \pm 0.009 (GeV^{-2})$	α'_f	$0.84 (GeV^{-2})$ (FIXED)
$r_{\mathbb{P}_1}^2$	$9.595 \pm 0.6289 (GeV^{-2})$	r_f^2	$41.424 \pm 7.971 (GeV^{-2})$
	Pomeron₂		ω-Reggeon
$\Delta_{\mathbb{P}_2}$	0.14437 ± 0.0051	Δ_ω	-0.53 (FIXED)
$c_{\mathbb{P}_2}$	6.87 ± 0.36	c_ω	-171.36 ± 8.23
$\alpha'_{\mathbb{P}_2}$	$0.082 \pm 0.004 (GeV^{-2})$	α'_ω	$0.93 (GeV^{-2})$ (FIXED)
$r_{\mathbb{P}_2}^2$	$4.765 \pm 0.2533 (GeV^{-2})$	r_ω^2	$2.621 \pm 6.362 (GeV^{-2})$
	Odderon		
$\Delta_{\mathbb{O}}$	-0.2707 ± 0.1178	s_0	$1.0 (GeV^2)$ (FIXED)
$c_{\mathbb{O}}$	1.8134 ± 1.4837		
$\alpha'_{\mathbb{O}}$	$0.029 \pm 0.023 (GeV^{-2})$		
$r_{\mathbb{O}}^2$	$1.159 \pm 0.591 (GeV^{-2})$		

Table 3: Parameters obtained by fitting to the data with two Pomeron contributions.

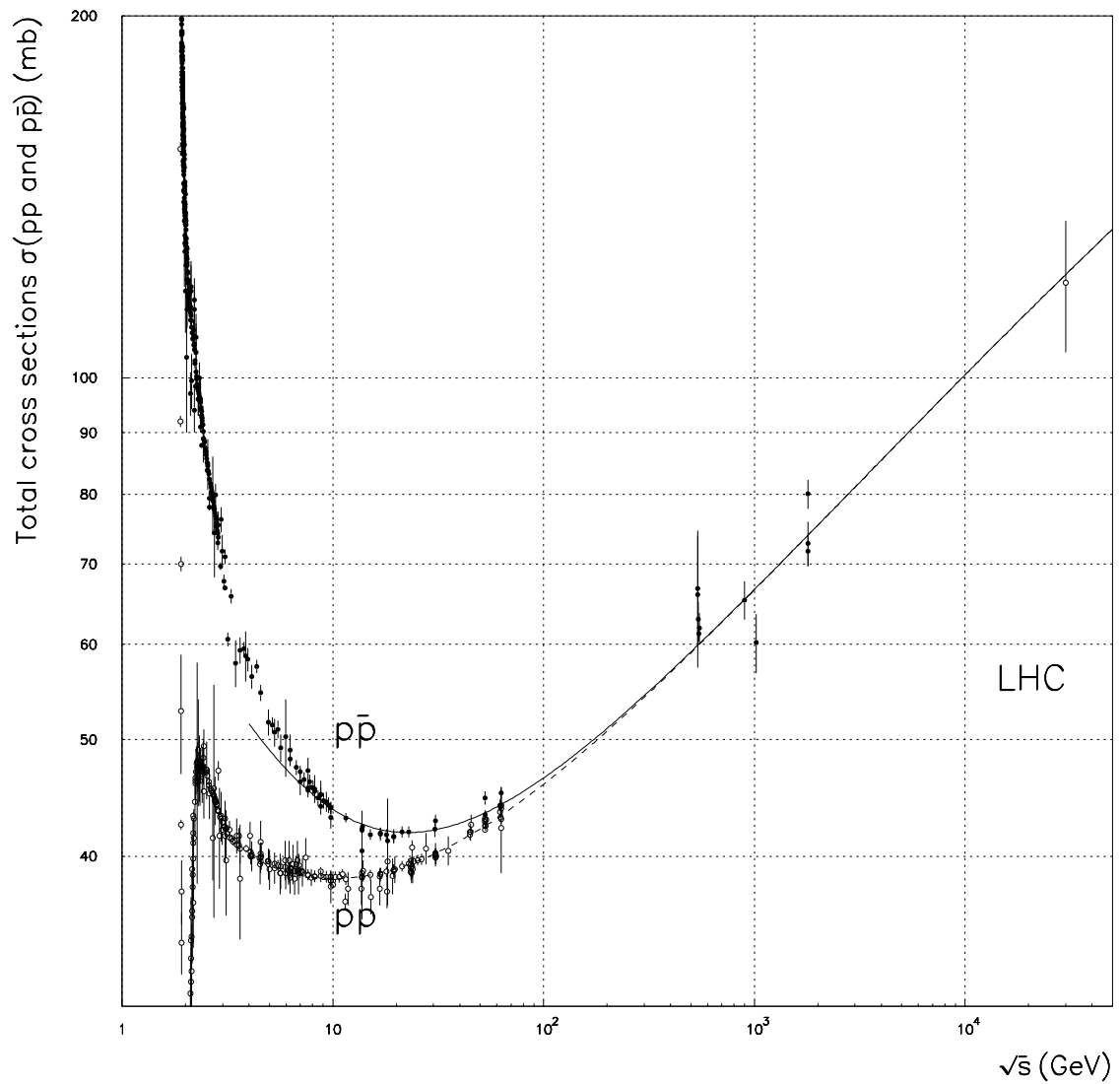


Figure 1: Total cross sections of pp scattering (hollow circles) and $\bar{p}p$ scattering (full circles) and curves corresponding to their description in the present model.

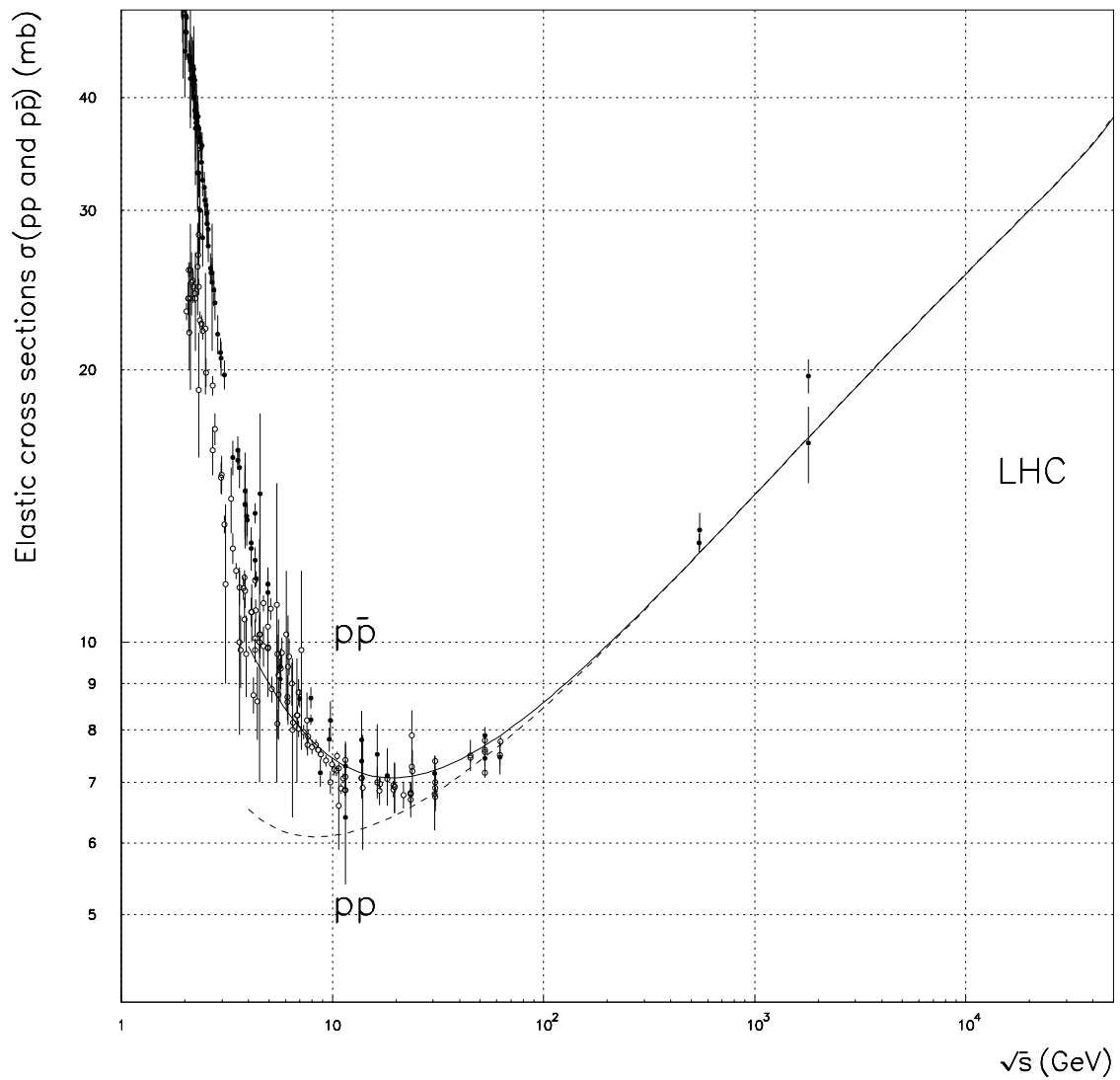


Figure 2: Elastic cross sections of pp scattering (hollow circles) and $\bar{p}p$ scattering (full circles) and curves corresponding to their description in the present model. These sets of data are not included in the fit.

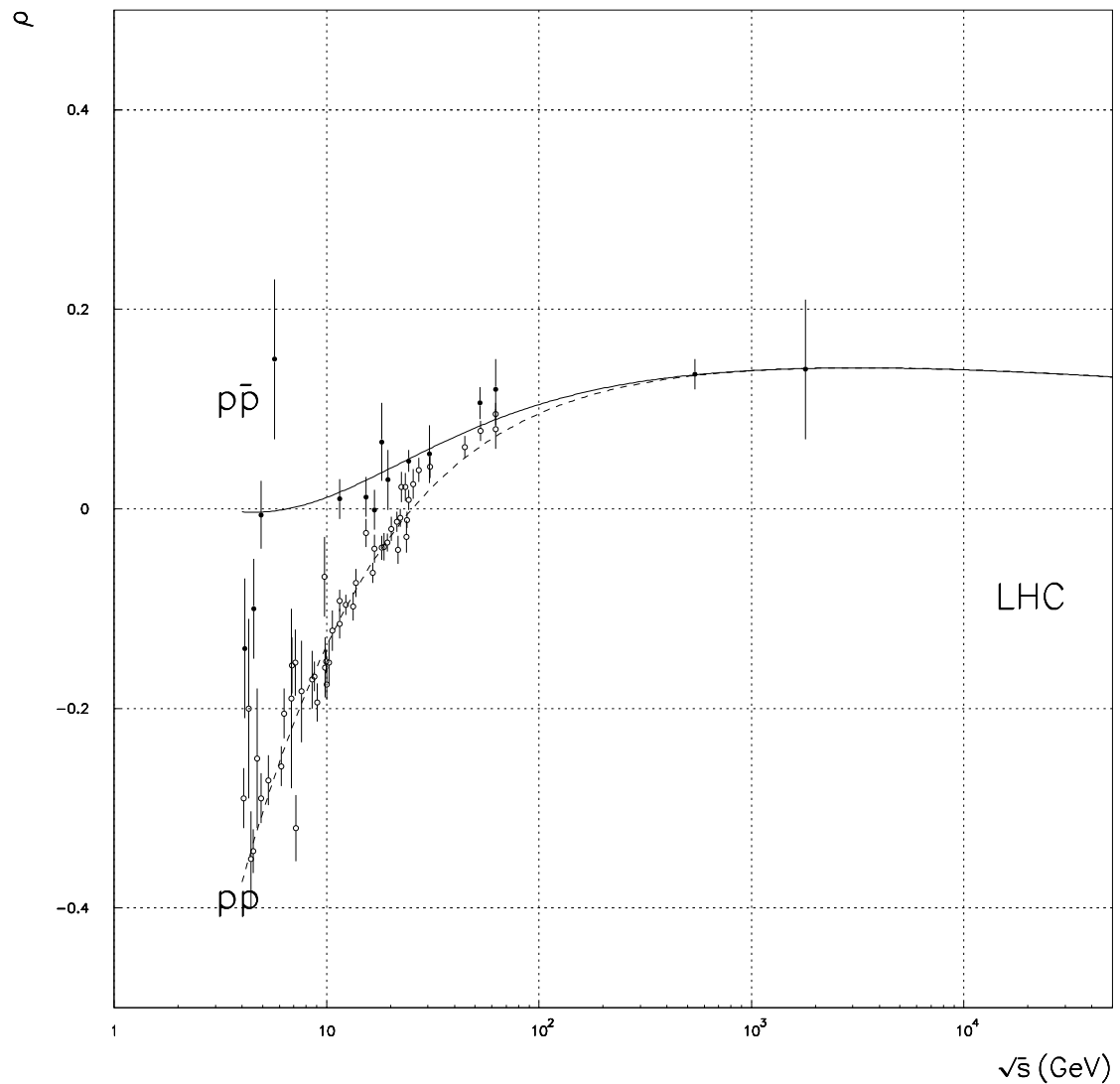


Figure 3: Ratios of the real to the imaginary part of the forward pp scattering amplitude (hollow circles) and $\bar{p}p$ scattering amplitude (full circles) and curves corresponding to their description in the present model.

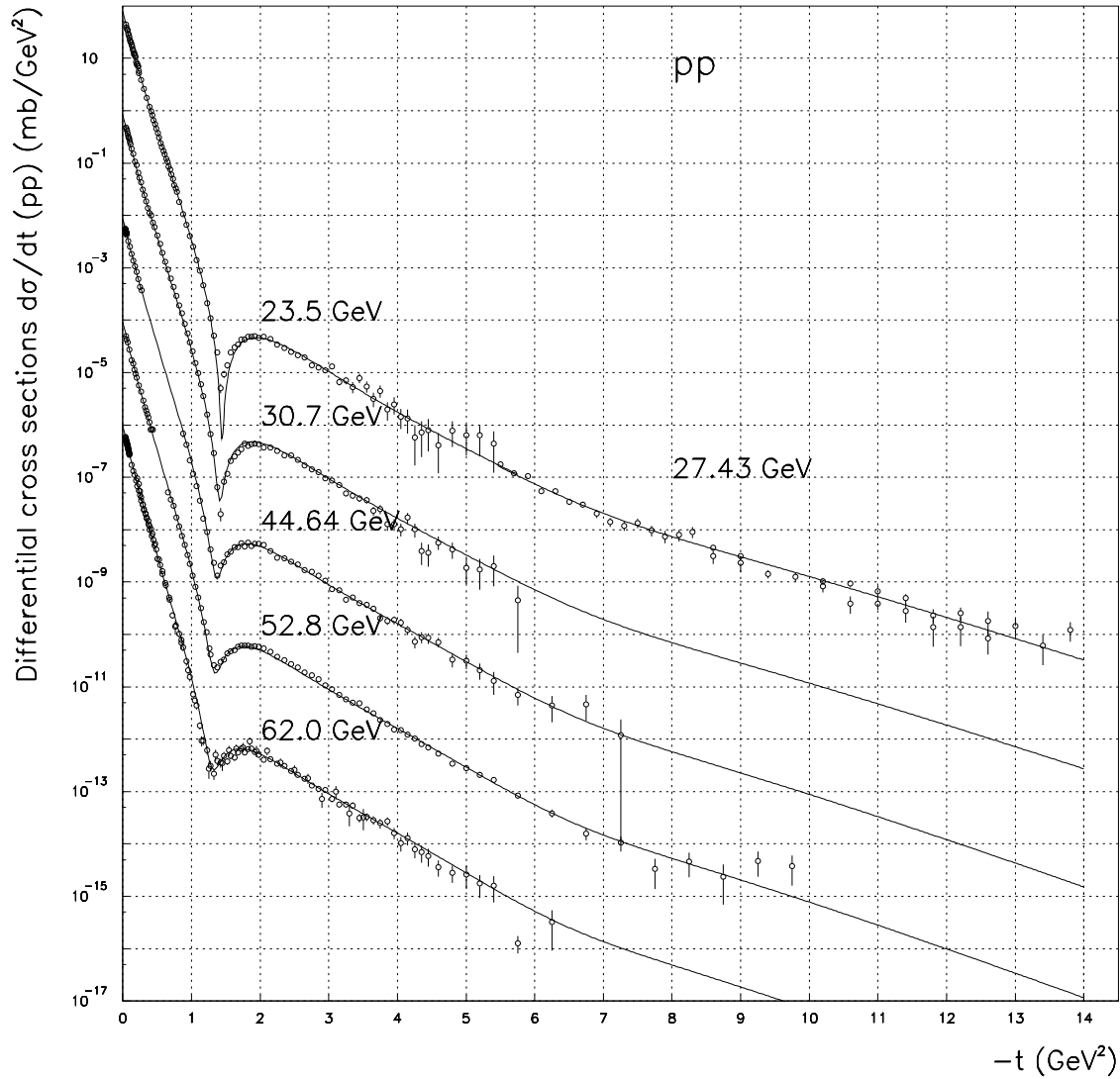


Figure 4: Differential cross-sections for pp scattering and curves corresponding to their description in the present model. A 10^{-2} factor between each successive set of data is omitted.

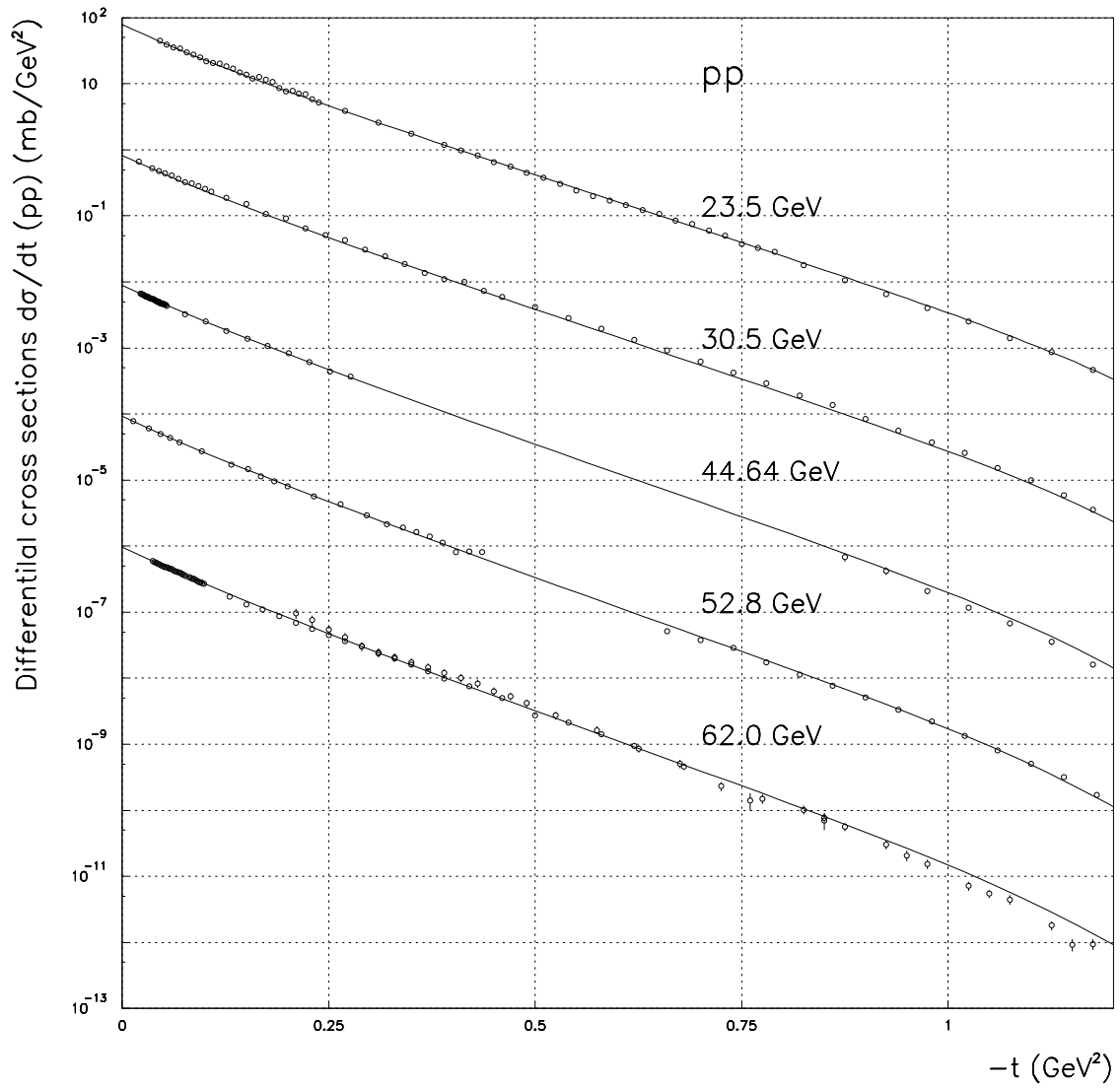


Figure 5: Differential cross-sections for pp scattering in the region of small momenta $0.01 \leq |t| \leq 1.2 \text{ GeV}^2$ and curves corresponding to their description in present the model. A 10^{-2} factor between each successive set of data is omitted.

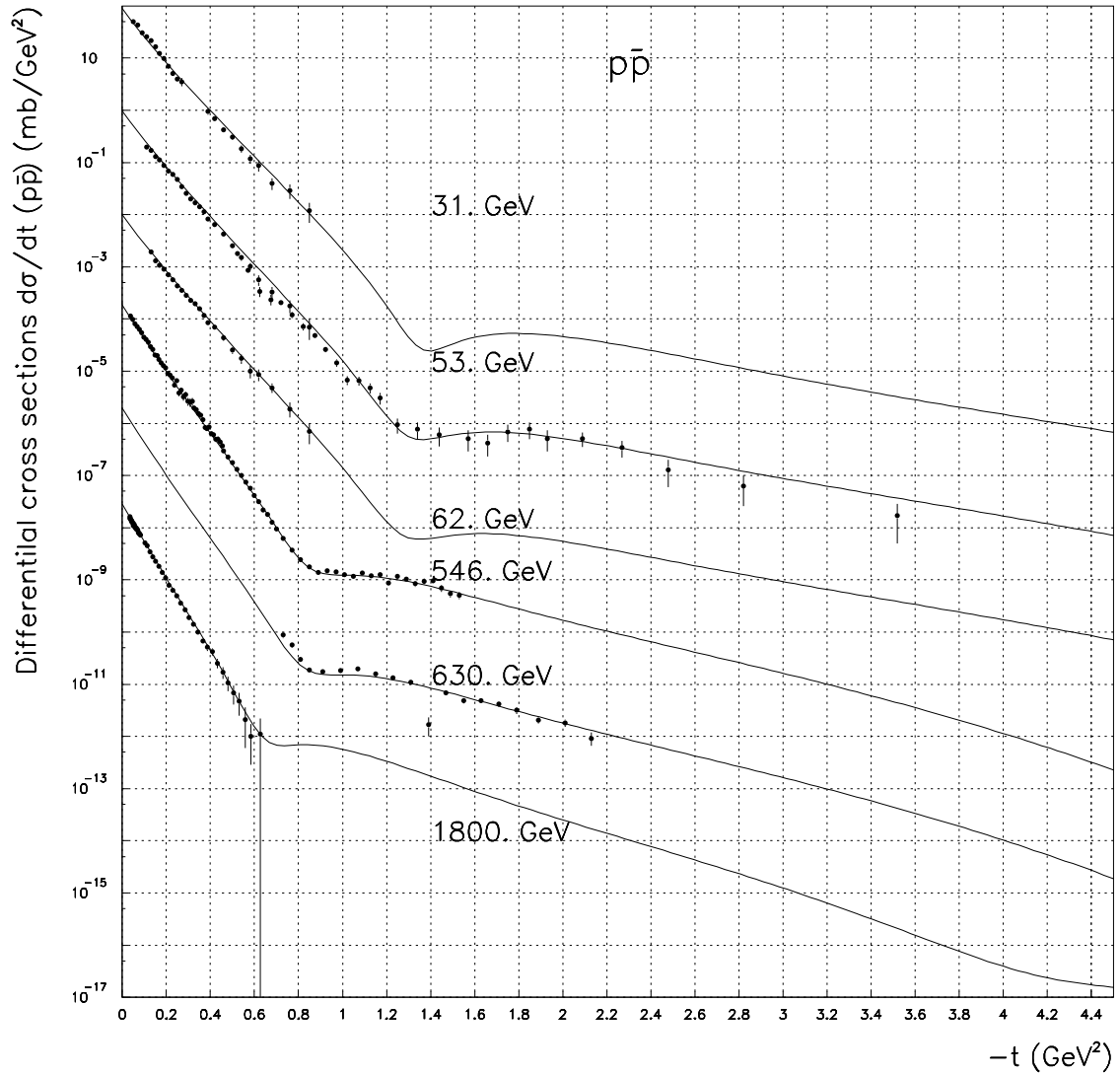


Figure 6: Differential cross-sections for $\bar{p}p$ scattering and curves corresponding to their description in the present model. A 10^{-2} factor between each successive set of data is omitted.

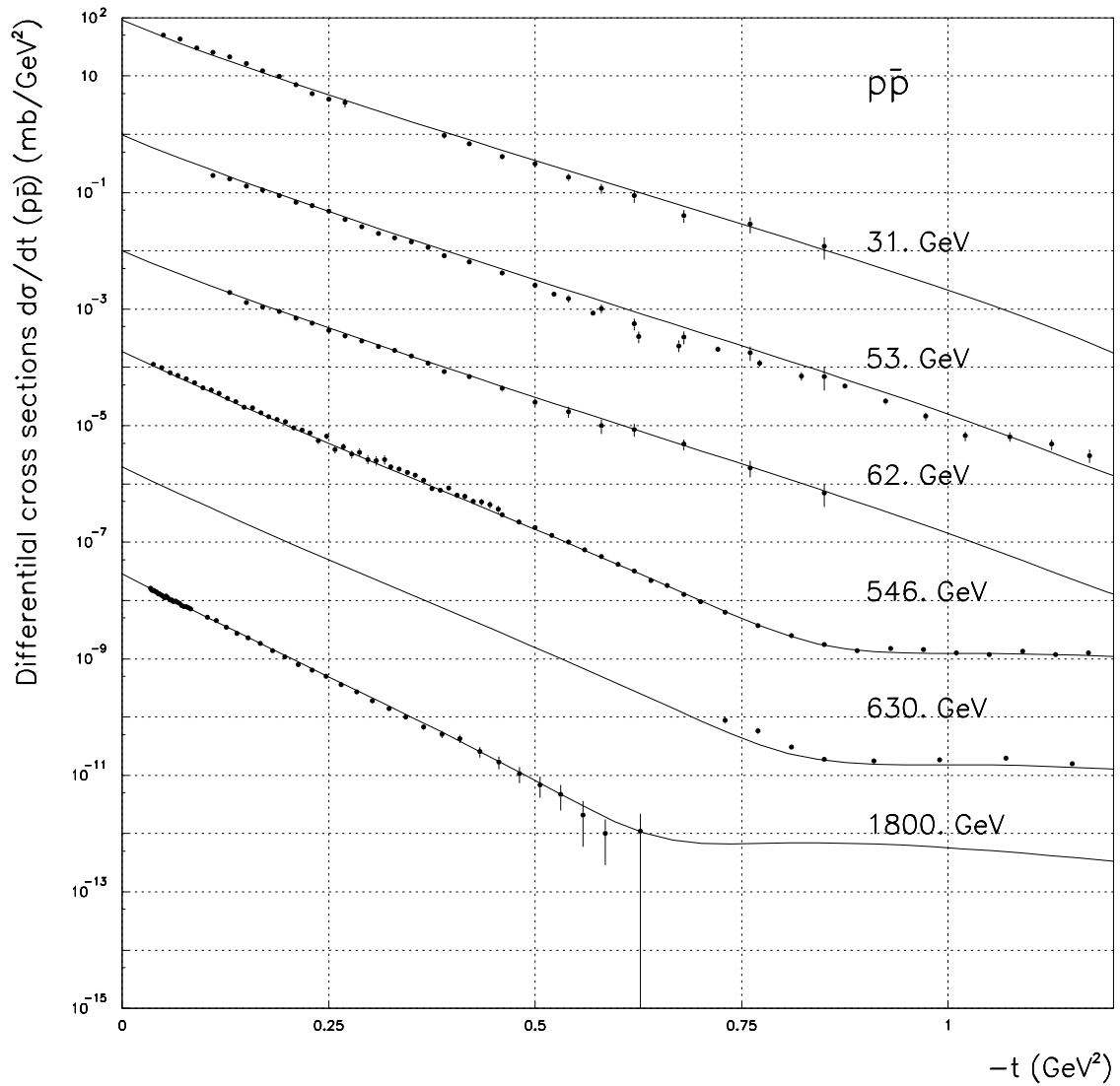


Figure 7: Differential cross-sections for pp scattering in the region of small momenta $0.01 \leq |t| \leq 1.2 \text{ GeV}^2$ and curves corresponding to their description in the present model. A 10^{-2} factor between each successive set of data is omitted.

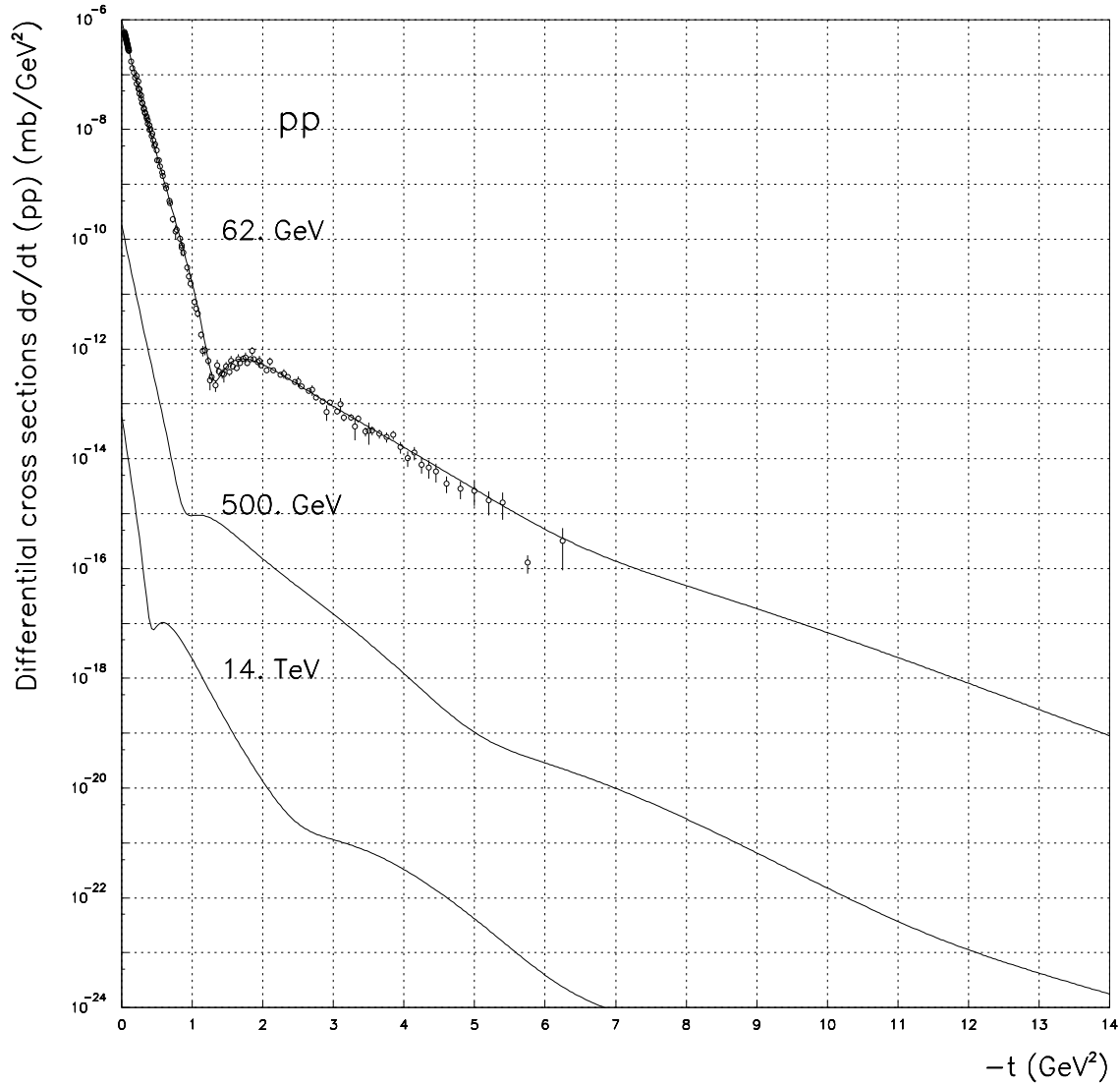


Figure 8: Predictions of the model for the differential cross-section of pp scattering which will be measured at LHC with $\sqrt{s} = 14. \text{TeV}$ and at RHIC $\sqrt{s} = 500. \text{GeV}$. The data corresponding to the energy $\sqrt{s} = 62. \text{GeV}$ is multiplied by 10^{-8} , RHIC by 10^{-12} , and that of LHC by 10^{-16} .

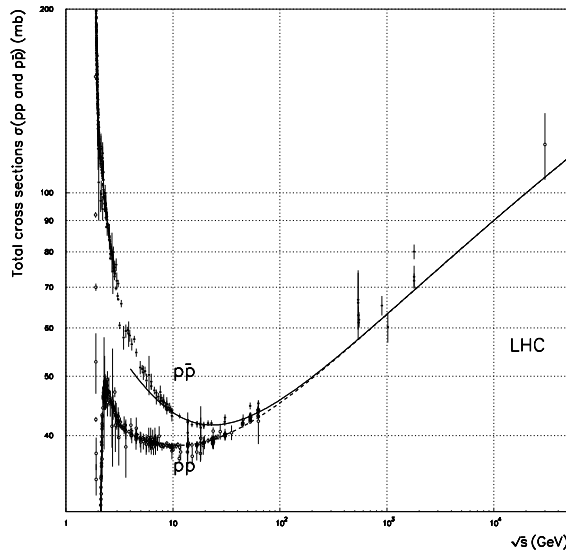


Figure 9: Total cross sections of pp scattering (hollow circles) and $\bar{p}p$ scattering (full circles) and curves corresponding to their description in the two-Pomeron model.

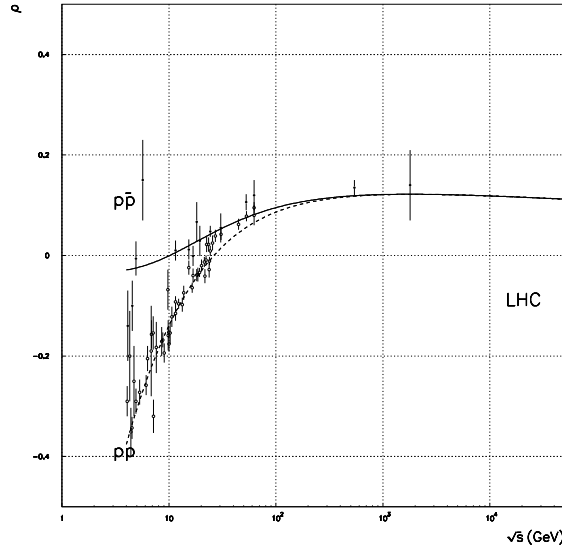


Figure 10: Ratios of the real to the imaginary part of the forward pp scattering amplitude (hollow circles) and $\bar{p}p$ scattering amplitude (full circles) and curves corresponding to their description in the two-Pomeron model.

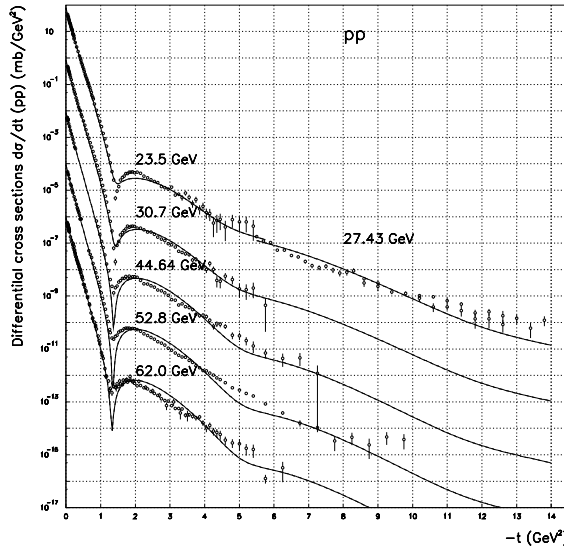


Figure 11: Differential cross-sections for pp scattering and curves corresponding to their description in the two-Pomeron model. A 10^{-2} factor between each successive set of data is omitted.

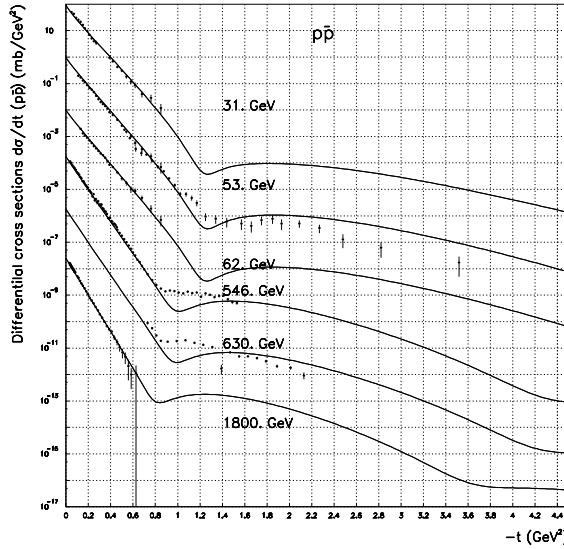


Figure 12: Differential cross-sections for $\bar{p}p$ scattering and curves corresponding to their description in the two-Pomeron model. A 10^{-2} factor between each successive set of data is omitted.

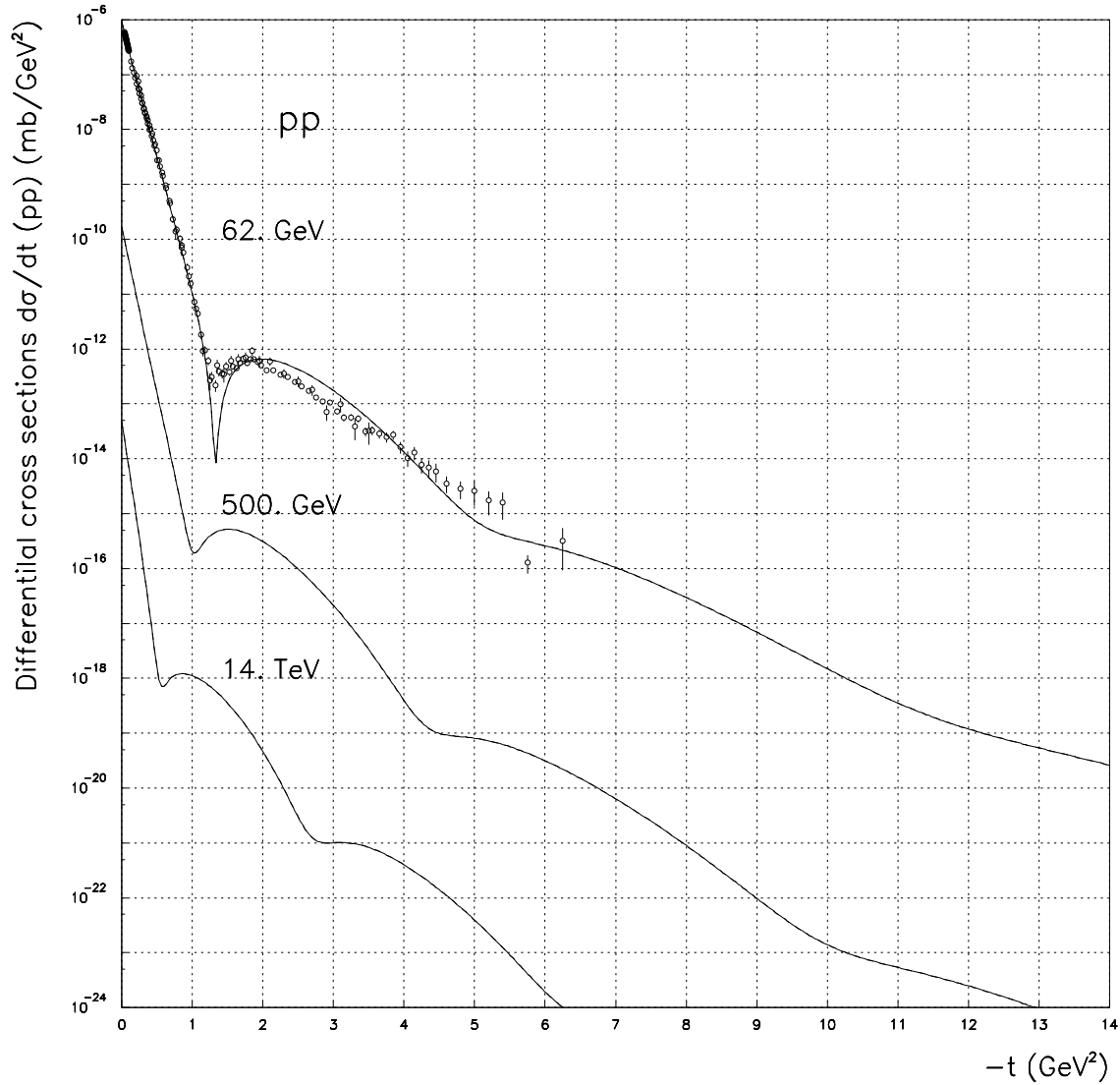


Figure 13: Predictions of the two-Pomeron model for the differential cross-section of pp scattering which will be measured at LHC with $\sqrt{s} = 14. \text{ TeV}$ and at RHIC $\sqrt{s} = 500. \text{ GeV}$. The data corresponding to the energy $\sqrt{s} = 62. \text{ GeV}$ is multiplied by 10^{-8} , RHIC by 10^{-12} , and that of LHC by 10^{-16} .

4 CONCLUSION AND DISCUSSION

Above we have developed a model which is based on a general argument of multiplicity of the Pomeron Regge poles in the eikonal. The present model shows a very good description of the available data for all momenta ($0.01 \leq |t| \leq 14. \text{ GeV}^2$) and energies ($8. \leq \sqrt{s} \leq 1800. \text{ GeV}$) so that $\chi^2/\text{d.o.f.} = 2.74$.

The model predicts the appearance of two dips in the differential cross-section which will be measured at LHC, fig. 8, and this prediction is stable in the sense that all two models with two and three Pomeron contributions predict the same behaviour of the differential cross-section with two dips. These dips are to appear in the region $t_1 \simeq -0.5 \text{ GeV}^2$ and $t_2 \simeq -2.5 \text{ GeV}^2$ which is in agreement with other predictions (model [6]).

We predict the following values of the total cross-section, elastic cross-section, and the ratio of real to imaginary part of the amplitude for the LHC:

$$\sqrt{s} = 14. \text{ TeV} ,$$

$$\sigma_{tot}^{pp} = 106.73 \text{ (mb)} \begin{array}{l} +7.56 \text{ mb} \\ -8.50 \text{ mb} \end{array} , \quad (17)$$

$$\sigma_{elastic}^{pp} = 29.19 \text{ (mb)} \begin{array}{l} +3.58 \text{ mb} \\ -2.83 \text{ mb} \end{array} ,$$

$$\rho^{pp} = 0.1378 \begin{array}{l} +0.0042 \\ -0.0612 \end{array} .$$

Predictions for RHIC are:

$$\sqrt{s} = 500. \text{ GeV} ,$$

$$\sigma_{tot}^{pp} = 59.05 \text{ (mb)} \begin{array}{l} +2.94 \text{ mb} \\ -3.10 \text{ mb} \end{array} , \quad (18)$$

$$\sigma_{elastic}^{pp} = 12.29 \text{ (mb)} \begin{array}{l} +0.79 \text{ mb} \\ -0.76 \text{ mb} \end{array} ,$$

$$\rho^{pp} = 0.1327 \begin{array}{l} +0.0052 \\ -0.0071 \end{array} .$$

The parameters of the Pomeron trajectories are:

$$\begin{aligned}\alpha(0)_{\mathbb{P}_1} &= 1.058, \quad \alpha'(0)_{\mathbb{P}_1} = 0.560 \text{ (GeV}^{-2}\text{)}; \\ \alpha(0)_{\mathbb{P}_2} &= 1.167, \quad \alpha'(0)_{\mathbb{P}_2} = 0.273 \text{ (GeV}^{-2}\text{)}; \\ \alpha(0)_{\mathbb{P}_3} &= 1.203, \quad \alpha'(0)_{\mathbb{P}_3} = 0.094 \text{ (GeV}^{-2}\text{)}.\end{aligned}\quad (19)$$

Their coupling constants fulfil the following inequality:

$$c_{\mathbb{P}_1} > c_{\mathbb{P}_2} > c_{\mathbb{P}_3} \quad (20)$$

It may mean that there exists a series of Pomeron contributions each term having the form (11), or these three contributions effectively emulate one nonlinear Pomeron trajectory.

The intercepts and slopes fulfil the following inequalities:

$$\begin{aligned}\Delta_{\mathbb{P}_1} &< \Delta_{\mathbb{P}_2} < \Delta_{\mathbb{P}_3} \\ \alpha'_{\mathbb{P}_1}(0) &> \alpha'_{\mathbb{P}_2}(0) > \alpha'_{\mathbb{P}_3}(0),\end{aligned}\quad (21)$$

i.e. the higher is the intercept the lower is the slope. We observe that the product of the intercept and the slope is approximately the same for all the Pomerons, $\Delta \cdot \alpha'(0) \simeq 0.040 \pm 0.0009 \text{ (GeV}^{-2}\text{)}$. This is seen in fig. 14. This constant seems surprisingly universal if compared with the products of other Reggeon parameters used in this model (fig. 15). At present we have no clear understanding of this universality.

We can only remind that high energy asymptotic behaviour of total and elastic cross-sections in Regge-eikonal approach have the following form:

$$\begin{aligned}\sigma_{tot}(s) \Big|_{s \rightarrow \infty} &\rightarrow 8\pi\alpha'_{\mathbb{P}}(0)\Delta_{\mathbb{P}} \ln^2(s/s_0), \\ \sigma_{elastic}(s) \Big|_{s \rightarrow \infty} &\rightarrow 4\pi\alpha'_{\mathbb{P}}(0)\Delta_{\mathbb{P}} \ln^2(s/s_0),\end{aligned}\quad (22)$$

and the constant $\alpha'_{\mathbb{P}}(0)\Delta_{\mathbb{P}}$ (GeV $^{-2}$) (there \mathbb{P} stands for the rightmost singularity of the eikonal function in J -plane) defines a universal (independent on colliding beams) asymptotic behaviour.

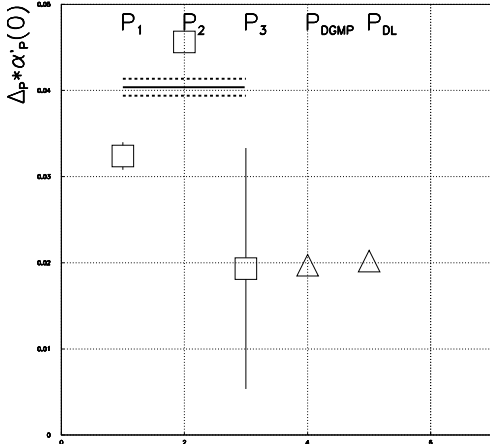


Figure 14: Products of intercepts to slopes for the Pomerons (hollow squares) and the Pomeron in a generalized eikonalization model \mathbb{P}_{DGMP} [6], Donnachie&Landshoff Supercritical Pomeron \mathbb{P}_{DL} [14] (hollow triangles). Solid line corresponds to the mean value of the product (for the three Pomerons) and dashed lines correspond to its error corridor.

It is interesting to enlist the following characteristic properties of the Pomerons used in this paper.

The first of the Pomerons ('Pomeron₁') possesses the properties that we expect from the string picture [15] of Reggeons, i.e. $\alpha'(0)_{\mathbb{P}} = \frac{1}{2}\alpha'(0)_f = 0.42 (GeV^{-2})$ and indeed $\alpha'(0)_{\mathbb{P}_1} = 0.559 \pm 0.078 (GeV^{-2})$.

The second Pomeron ('Pomeron₂') is close to what is called "supercritical Pomeron" with the slope $\alpha'(0)_{\mathbb{P}_2} = 0.273 \pm 0.005 (GeV^{-2})$ close to its "world" value $\alpha'(0)_{\mathbb{P}} \simeq 0.25 (GeV^{-2})$.

The third Pomeron ('Pomeron₃') is reminiscent of what is known as a

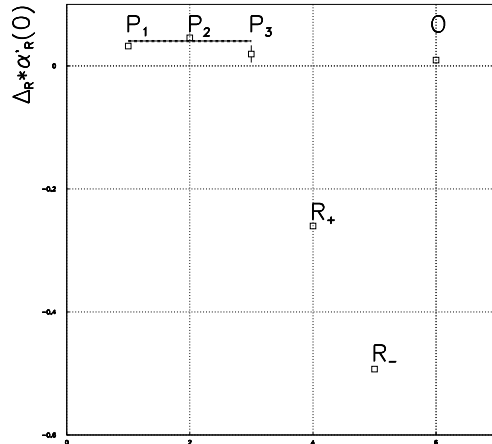


Figure 15: Products of intercepts to slopes for the Pomerons, the Odderon, and Reggeons used in the present model.

“hard” (or perturbative QCD)Pomeron. Its parameters ($\alpha(0)_{\mathbb{P}_3} = 1.203$, $\alpha'(0)_{\mathbb{P}_3} = 0.094 (GeV^{-2})$) are close to the calculated parameters of the perturbative Pomeron, which arise from the summation of reggeized gluon ladders and BFKL equation [16]: $\alpha(0)_{\mathbb{P}}^{BFKL} \simeq 1.2$, $\alpha'(0)_{\mathbb{P}}^{BFKL} \sim 0. (GeV^{-2})$. The fact of arising of a “hard” Pomeron in a presumably “soft” framework can seem quite unexpected. However we are not particularly inclined to identify straightforwardly “our hard Pomeron” with that which is a subject of perturbative QCD studies.

The Odderon has the following parameters: $\alpha(0)_{\mathbb{O}} = 1.192$, $\alpha'(0)_{\mathbb{O}} = 0.048 (GeV^{-2})$ in agreement with unitarity constraints Eq. (15). The Odderon intercept is positive and close to that of the $Pomeron_3$. The slope is almost zero. The coupling is so small that only high-t data may be sensible to the Odderon contribution.

Assuming that one can neglect the non-linearities of Regge trajectories and making use of a simple parametrization

$$\alpha(m^2) = \alpha(0) + \alpha'(0) \cdot m^2, \quad (23)$$

we can try to estimate the corresponding spectroscopic content of our model.

Then $\Re\alpha(m^2) = J$, where J is an integer number corresponding to the spin of a particle which we should find lying on the trajectory.

The trajectories are depicted in fig. 16. The $C+$ Reggeon trajectory is in fact a combination of two families of mesons f and a_2 . The $C-$ Reggeon trajectory is a combination of two families of mesons ω and ρ . As is seen, the secondary Reggeon trajectories fairly well describe the spectrum of mesons.

Among the mesons with appropriate quantum numbers there exists two that fit the Pomeron trajectory (0^+J^{++}): $f_2(1810)$ 0^+2^{++} with mass $m = 1815 \pm 12$ MeV and $X(1900)$ 0^+2^{++} with mass $m = 1926 \pm 12$ MeV. One of them is supposed to be on $Pomeron_2$ trajectory.

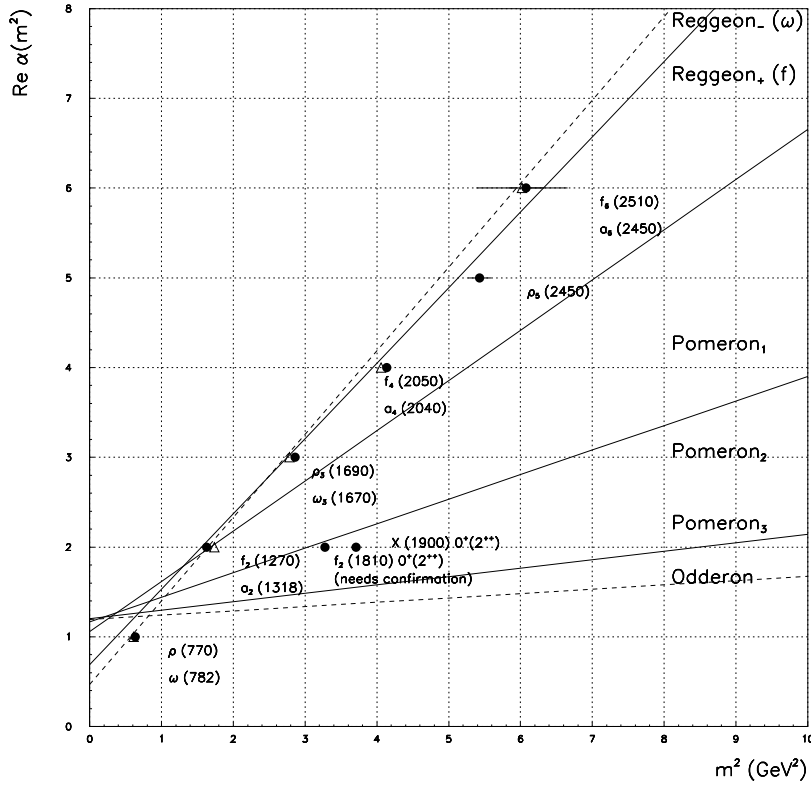


Figure 16: Regge trajectories of secondary Reggeons, three Pomerons and the Odderon.

ACKNOWLEDGMENTS

We would like to thank professor Enrico Predazzi for useful discussions and for reading the manuscript.

References

- [1] V.A. Petrov, A.V. Prokudin, S. M. Troshin and N. E. Tyurin, hep-ph/0103257; subm. to *Journal of Physics G*.
- [2] A. Faus-Golfe, J. Velasco and M. Haguenauer, hep-ex/0102011.
- [3] Pierre Gauron and Basarab Nicolescu, *Phys. Lett. B* **486**, 71 (2000), hep-ph/0004066;
- [4] K. Kontros, A. Lengyel and Z. Tarics, hep-ph/0011398
- [5] A. Donnachie, P. V. Landshoff, *Phys. Lett. B* **437**, 408 (1998);
- [6] P. Desgrolard, M. Giffon, E. Martynov, E. Predazzi *Eur.Phys.J. C* **C16**, 499-511 (2000)
- [7] M. M. Block, E. M. Gregores, F. Halzen, G. Pancheri *Phys. Rev. Lett.* **D60**, 054024 (1999)
- [8] A. K. Likhoded and O. P. Yushchenko, *Int. Jour. of Mod. Phys. A* **6**, 913 (1991).
- [9] L. N. Lipatov, *Yad. Fiz.* **23**, 642 (1976).
- [10] V. A. Petrov, A. V. Prokudin, in the Proceedings of the International Conference on Elastic and Diffractive Scattering (VIIIth ‘Blois Workshop’) June 28 - July 2, 1999 Protvino, Russia, World Scientific Publishing 2000, Singapore 2000, p. 95. hep-ph/9912245
- [11] R. J. M. Covolan, P. Desgrolard, M. Giffon, L. L. Jenkovszky, E. Predazzi, *Z. Phys. C* **58**, 109 (1993)
- [12] M. Froissart, *Phys. Rev. D* **123**, 1053 (1961);
A. Martin, *Phys. Rev. D* **129**, 993 (1963).
- [13] M. Giffon, E. Martynov, E. Predazzi, *Z. Phys. C* **76**, 155 (1997);
J. Finkelstein, H. M. Fried, K. Kang, C. -I. Tan, *Nucl. Phys. B* **232**, 257 (1989);
E. Martynov *Phys. Lett. B* **267**, 257 (1989);
H. M. Fried, in “Functional Methods and Eikonal Models” (Editions Frontières, 1990) p. 214.

- [14] A. Donnachie, P. V. Landshoff, *Phys. Lett. B* **296**, 227 (1992)
- [15] L. D. Soloviev, preprint IHEP 2000-20, Protvino 2000 (in Russian); hep-ph/0006010; subm. to *Theor. and Math. Phys.*.
- [16] V. S. Fadin, L. N. Lipatov, *Phys. Lett. B* **429**, 127 (1998);
Marcello Ciafaloni, Gianni Camici, *Phys. Lett. B* **430**, 349 (1998);
D. A. Ross, *Phys. Lett. B* **431**, 161 (1998).